EES Solar

PAPER

View Article Online
View Journal | View Issue

Cite this: *EES Sol.*, 2026, **2**, 161

Enhanced mechanical load testing of photovoltaic modules for cold and snowy climates

Anika Gassner, *[ab] Gabriele C. Eder,[a] Ebrar Özkalay,[c] Gabi Friesen,[c] Markus Feichtner[d] and Vasiliki-Maria Archodoulaki[b]

Photovoltaic (PV) deployment is increasing rapidly and even expanding into cold and snowy climates, where harsh conditions – strong winds, heavy snowloads, sub-zero temperatures, and temperature fluctuations – pose reliability challenges for PV modules. Climate-adapted accelerated aging tests are required to evaluate and choose modules capable of withstanding such climate conditions. This study investigated the mechanical stability of PV modules featuring different designs and materials at varying temperatures. Tests were performed on materials, mini modules, and full-size modules, focusing on the impact of the encapsulant behavior at low temperatures on the mechanical stability of the solar cells and glass of the module laminates. Mini modules results showed that polyolefin-based (POE) encapsulants remain flexible at low temperatures and offer better protection against mechanical damage than ethylene vinyl acetate (EVA) encapsulants. For full-size glass/backsheet modules with busbar metallization, mechanical load (ML) testing at −40 °C, and ML at 25 °C after thermal pre-stressing, resulted in increased cell cracking compared to standard ML tests at 25 °C. In contrast, thinner multi-wire metallization or a glass/glass structure – which demonstrated enhanced structural integrity – reduced cell cracking under loads. However, glass thickness and clamping of the frameless modules limited resistance to higher pressure. These findings highlight the importance of climate-specific testing and optimized material selection and module design to ensure PV system durability in cold and snowy climates.

Received 5th August 2025
Accepted 6th October 2025

DOI: 10.1039/d5el00125k

rsc.li/EESSolar

Broder context

As the global demand for clean and reliable energy solutions grows, photovoltaic (PV) technology has become essential to the transition toward renewable energy and climate change mitigation. Today, PV technology is one of the most affordable energy sources worldwide and plays a crucial role in reducing reliance on fossil fuels. This progress enables the expansion of PV deployment into regions with harsher climates, where access to clean energy sources is equally critical. In cold and snowy regions, for example, PV modules must withstand high snow and wind loads as well as low temperatures. Climate-specific stress testing is therefore essential to guide the development of more robust module designs. This study evaluates the mechanical stability of mini and full-size modules featuring various encapsulant materials and design configurations, focusing particularly on module performance during mechanical load tests at low temperatures and following thermal cycling. Results show that polyolefin encapsulants maintain their elasticity in cold conditions, offering improved cell protection under mechanical loads. Glass/glass module structures provide greater structural integrity, and modules with thicker glass and frames demonstrate superior load-bearing capacity. These findings support more reliable material and design strategies for PV deployment in cold climate regions.

1 Introduction

The photovoltaic (PV) industry is currently entering the multi-terawatt era, driven primarily by significant cost reductions and the urgent need to generate electricity from renewable energy sources. This transition has facilitated the deployment of PV systems in areas previously deemed too costly or insignificant, such as cold and snowy regions either at higher latitudes or altitudes.[1] For instance, alpine countries like Austria and Switzerland are increasingly ramping up efforts to install PV systems in mountainous regions. Such systems show higher yields,[2] lower degradation rates,[3] and enhanced winter electricity production compared to lowland systems.[4,5] Furthermore, PV systems can be attached or integrated into alpine infrastructure to supply power to remote consumers, such as mountain huts and ski areas, or in conjunction with hydroelectric power plants. Additionally, interest in larger freestanding PV systems or modules integrated into the built environment has grown in high latitude regions due to long summer daylight hours and advantageous colder operating temperatures.[6,7]

[a]*OFI Austrian Research Institute for Chemistry and Technology, Franz Grill Str. 5, 1030, Vienna, Austria. E-mail: anika.gassner@ofi.at*

[b]*TU Wien, Institute of Materials Science and Technology, Vienna, Austria*

[c]*University of Applied Sciences and Arts of Southern Switzerland (SUPSI), Mendrisio, Switzerland*

[d]*Sonnenkraft Energy GmbH, St.Veit a.d. Glan, Austria*

The deployment of PV systems in cold and snowy climates requires the adaptation of PV modules and components to withstand more severe environmental conditions and stressors. Especially single but repeated weather events, such as heavy snowfall, strong wind gusts, or ice formation, can impact the durability and longevity of PV modules and systems.[1] Moreover, continuous stressors at high-altitudes, such as higher irradiance, low temperatures, and rapid temperature fluctuations, can affect the stability of materials and components used in the modules and systems, potentially leading to degradation or failure (see Fig. 1).[8–11] To ensure reliable and sustainable operation of PV installations in these climates, it is essential that systems currently being planned and soon to be constructed are designed to withstand these challenges.[12] This includes the multi-material laminates (PV modules), fasteners, and mounting structures.

Until recently, all module types – regardless of their targeted installation under specific climatic conditions, operating environments, or applications – were tested and certified according to the same general test procedures outlined in IEC 61215[13] and IEC 61730.[14] However, this approach has been evolving recently, with the introduction of new technical guidelines and standards in recent years to address more specific requirements, such as IEC TS 63126[15] for modules operating at elevated temperatures, IEC 62892:2019[16] for faster temperature fluctuations, IEC 62938:2020[17] for uneven snow loads, or IEC TS 63397:2022[18] for increased hail frequency. However, test methods for specific operating conditions, such as cold temperatures and snow, are still lacking. Existing testing strategies, especially those regarding mechanical resistance, must be further developed to identify and optimize the most suitable module designs and materials for such demanding climatic conditions.

Because mechanical stress from snow, ice, and wind load is a prevalent source of damage to PV systems in cold and snowy climates, these stress factors must be given special consideration in accelerated aging tests. At low temperatures, which frequently occur in such environments, the structural properties of polymeric materials or material combinations can be significantly affected. In particular, polymers frequently used as encapsulation may approach or fall below their glass transition temperature (T_g), which results in increased stiffness due to a decreased polymer chain molecular mobility. This increased stiffness reduces the encapsulant's damping behavior, resulting in easier transfer of loads to the solar cells.[19,20] This increases the risk of solar cell cracks, metallization damage, and delamination.[21–23]

This study investigated different testing strategies – ranging from material tests of encapsulants over mini-modules to full-size PV modules – to support the discussion on which module designs and bills of materials (BoM) are best suited for deployment in the harsh conditions of cold and snowy climates. It also compared various testing approaches and outlines how standardized tests should be adapted for modules suited for installation in cold and snowy climates. Different material combinations and module designs are evaluated through highly accelerated aging tests, with the resulting electrical power losses analyzed in relation to damage. These results can be considered as a guideline for the product development of innovative, highly stable, and reliable PV modules for alpine or nordic use.

2 Methods and samples

To determine the optimal module design for a cold and snowy climate, several tests were conducted: starting from material level, through mini modules to full-size modules (Fig. 2). First, the thermomechanical and thermal behavior of the encapsulant materials was investigated. Then the impact of this behavior on the mechanical strength of mini- and full-size modules at different temperatures was tested. The following sections contain detailed descriptions of each step and the rationale behind the workflow.

2.1 Encapsulant material analysis

The structural, thermo-mechanical and thermal characteristics of encapsulant materials are of high importance when selecting the optimal BoM for modules for use in cold and snowy climates. To evaluate the materials, four different types of encapsulant films were characterized and compared (Fig. 3):

- Ethylene vinyl acetate (EVA) – from First type F406PS.
- Polyolefin (POE) – from First type TF4.

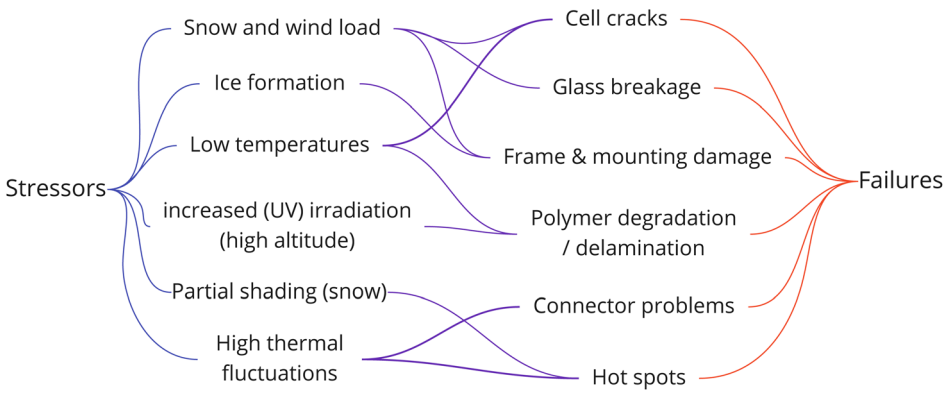

Fig. 1 Most typical stressors and the resulting failures in cold and snowy climate, adapted with permission.[1]

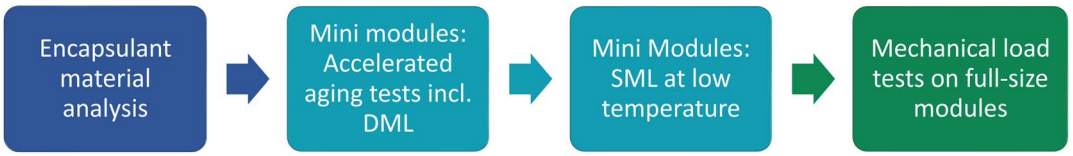

Fig. 2 Schematic overview of the testing procedure. (DML: dynamic mechanical load; SML: static mechanical load).

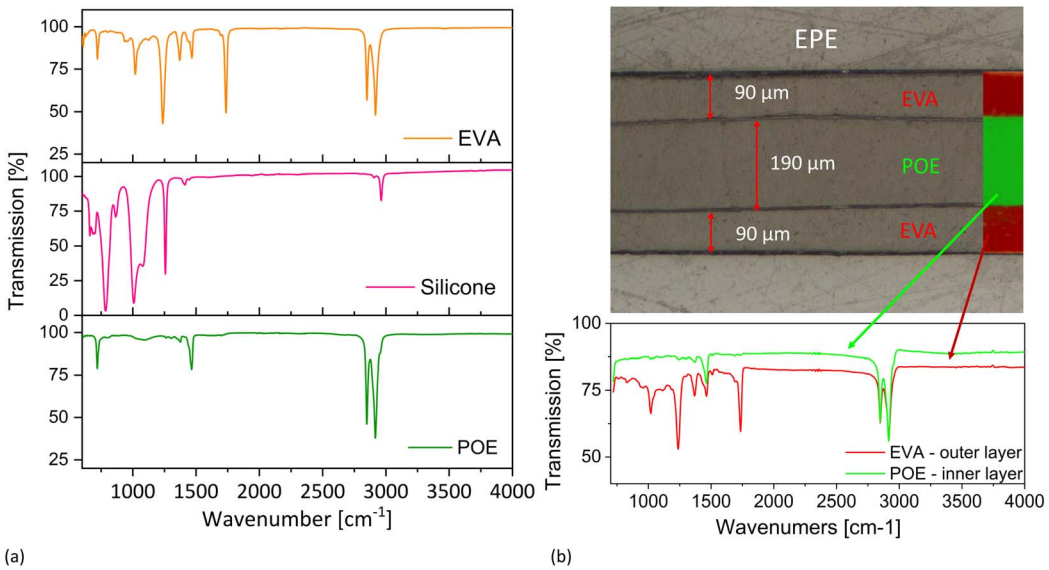

Fig. 3 (a) IR spectra of tested encapsulant materials EVA, Silicone and POE. (b) Light microscopic image with an inserted ATR-IR-image of the cross-section of EPE and extracted IR spectra of the layers.

- Silicone elastomer – from Dow type PV-6326.
- EPE (a three-layer structure consisting of EVA–POE–EVA – see Fig. 3b) – from FilmTec Solar type Protec EPE.

All encapsulants were examined in their cured (crosslinked) state to best replicate the conditions within a laminated PV module. The chemical identity/structure of the encapsulant films was determined *via* their infrared (IR) spectra (Fig. 3a). This analysis revealed that POE is a pure polyethylene based material and the silicone is a polydimethylsiloxane elastomer. An Fourier Transform Infrared spectrometer (PerkinElmer Frontier) and microscope (PerkinElmer Spotlight 400) were used for the attenuated total reflection point and imaging measurements, respectively.

The glass transition temperatures of the encapsulants were determined using differential scanning calorimetry (DSC) according to ISO 11357-2, performed with a Mettler Toledo DSC in nitrogen atmosphere. A heating rate of 20 K min^{-1} was used in a temperature range of −80 °C to 280 °C. In addition, a dynamic mechanical analysis (DMA) of the various encapsulant materials was performed according to ISO 6721-4. A Mettler Toledo DMA/SDTA 861 was used to analyze the thermomechanical properties of EVA, POE, and EPE. The temperature range was −60 °C to 80 °C, with a heating rate of 2 K min^{-1} and a frequency of 1 Hz.

In order to test the mechanical characteristics, tensile strength measurements were carried out according to ISO 527-3 (five-fold determination) in a temperature range from −40 °C to +50 °C, in increments of 10 °C. Due to the high flexibility of the encapsulant materials, no breakage was observed even at high elongation. Therefore, the tensile stress at 10% elongation was used for comparison between the different encapsulant materials as it reflects the strain levels during bending in a PV module.

2.2 Mini modules

To transfer the findings of the encapsulant material analysis to module laminates, in the next step the currently most frequently used encapsulation materials (EVA and POE) were evaluated within different module configurations: glass/glass (G/G) and glass/backsheet (G/BS). The aim was to compare the thermomechanical stability and the probability of failures of these combinations. For this purpose, four-cell mini modules were manufactured, each using 4 mm thick solar glass and full passivated emitter and rear contact (PERC) solar cells with five busbars. The back cover was either (i) glass or (ii) a polymeric backsheet composed of polyethylene terephthalate (PET) or polyvinyl fluoride (PVF)/PET/PVF, referred to as Tedlar-BS hereafter.

2.2.1 Accelerated aging tests on mini modules including dynamic mechanical loading. The thermomechanical stability of the mini-modules was assessed through a preliminary study using four cycles of an accelerated aging test sequence, as depicted in Fig. 4. This sequence involved temperature cycling

(TC), damp heat (DH), and irradiance (IRR). This series of tests was designed as a screening method to identify early on the impact of variations in structure and material on the stability of the modules under various accelerated test conditions. Thus, a broad spectrum of potential aging mechanisms was covered. The tests were conducted in a climate chamber equipped with metal halide lamps serving as an artificial sunlight source best suited for large area illumination.[24] The irradiance was set to 1200 Wm^{-2} to mimic typical conditions at high altitudes.[3,8] The TC test was conducted at a higher maximum temperature (100 °C) than given in IEC 61215. According to standard IEC 62892:2019 (ref. 16) the maximum temperature of the TC test can be increased up to 110 °C to increase the stress level or reduce the number of TC test cycles. For all three test stages of the sequence, a test duration of 100 hours was chosen to allow for a rapid assessment of the effects of the various stress factors. The dynamic mechanical load (DML) test was performed using a three-point bending setup on a dynamic testing machine PA40-280 from Form + Test. A total of 1000 cycles at 0.25 Hz with a load of 200 N (equivalent to a pressure of 1950 Pa on the module area) were applied. The module deflection was recorded during the test by the testing machine. Besides visual inspection to detect obvious failures, electroluminescence (EL) imaging of the mini-modules was performed between and after the tests to identify cell crack formation or damage of the cell metallization. A modified Sony A7S camera was used to take the images of the modules in the dark with the short circuit current applied. Additionally, electrical measurements were conducted before and after the tests to evaluate changes in electrical performance. The current–voltage (*I–V*) curves of modules were measured under standard testing conditions (STC), which are defined as module temperature of 25 °C, 1000 Wm^{-2} irradiance, and an air mass of 1.5 (AM1.5). These measurements were taken at an ISO 17025 accredited PV module testing laboratory using a class A+A+A+ 10 millisecond pulsed solar simulator (Pasan IIIb) with an uncertainty of ± 2.6%.

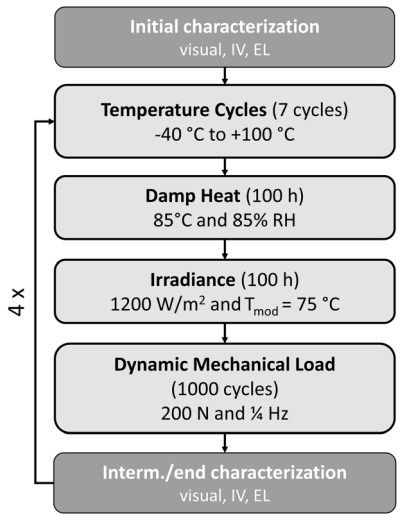

Fig. 4 Accelerated test sequence for the mini modules, including the dynamic mechanical load testing (EL: Electroluminescence, *IV*: current–voltage curve).

2.2.2 Static mechanical load testing at low temperature. To obtain more detailed results regarding the temperature influence on the mechanical stability of the two module structures (G/G *versus* G/BS) and the impact of the encapsulant type (EVA *versus* POE), static mechanical load tests (SML) were performed at different temperatures inside a climate chamber. The influence of low temperatures on the physical state of the encapsulation material and the resulting development of various failure modes (*e.g.* cell cracks or metallization damage) was assessed. A three-point bending test was again applied to the mini modules (Fig. 5). A load of 5400 Pa was applied for one hour at each temperature: initially at 20 °C, then at 0 °C, and subsequently decreased in 10 °C increments to −50 °C. The chosen load level was selected to identify differences between the various module designs and represents a typical test load for modules intended for use in areas with high snow and wind loads. The one-hour test duration is in accordance with IEC 61215 MQT 16,[13] as it can be assumed that the load and temperature have stabilized within this time span. EL images were captured at each temperature to detect the potential formation of new cell cracks or solder bond failures.

2.3 Mechanical load tests on full-size modules

The mechanical behavior of a PV module depends on its size.[25] Furthermore, the impact of the frame and the mounting clamps cannot be accurately assessed using mini modules. Thus, a holistic test setup was developed to analyze the effect of temperature and mechanical load (ML) on full-size PV modules. Different module designs – frameless G/G and framed G/BS – were tested using a specifically designed test sequence.

2.3.1 Samples. Table 1 summarizes the samples investigated, comparing framed G/BS modules with frameless G/G modules. It lists the glass thicknesses, cell and encapsulant types, and module dimensions. The PET backsheet has a thickness of 170 μm. The bifacial full PERC cells have five busbars. Due to the recent rapid technological changes in the solar industry, tests on PV modules containing half-cut Tunnel Oxide Passivated Contact (TOPCon) solar cells with 16 multi-wires were also added to the test program for comparison. In

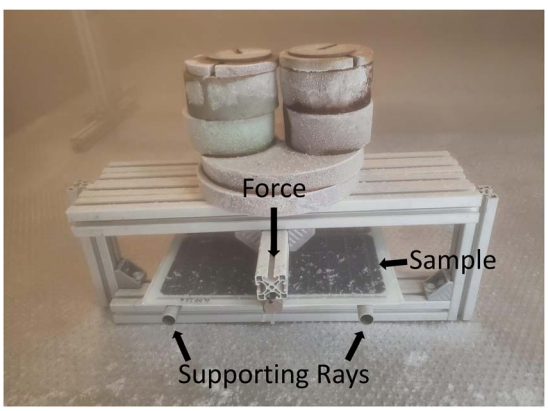

Fig. 5 3-Point bending test with a load of 5400 Pa on a mini module inside the climate chamber. Picture taken at −30 °C.

Table 1 Configurations of the full-size modules used for ML testing

Configuration	Glass thickness	Frame	Encapsulant	Cell type	Metallization	Dimensions [mm × mm]
G/G	6 mm/6 mm	No	EVA	PERC full	Busbar	2020 × 1015
G/G	4 mm/4 mm	No	EVA	PERC full	Busbar	1700 × 995
G/G	3 mm/3 mm	No	EVA	PERC full	Busbar	1700 × 995
G/BS	4 mm/PET-BS	Yes – 40 mm	EVA	PERC full	Busbar	1680 × 1015
G/BS	3.2 mm/PET-BS	Yes – 35 mm	EVA/POE/EPE	TOPCon half-cut	Multi-wire	1748 × 1143

addition to EVA, in these samples POE and the emerging EPE were also tested.

To minimize the influence of mounting variations on the results, it was ensured that the mounting configurations were as consistent as possible across all samples during the mechanical load tests. The G/G modules were mounted on an aluminum frame using three clamps (100 mm long) on each long side (six in total), simulating a mounting configuration without rails shading the back of the bifacial modules. The clamps were tightened to 15 Nm – as specified by the manufacturer – ensuring optimal mounting conditions. For the G/BS modules, six clamps were also used, this time attached to three mounting rails. The G/BS module with PERC cells is specified for high loads up to 7000 Pa in this configuration and includes special back rails designed to reinforce the frame.[26]

2.3.2 Mechanical load test flow. A specific test flow was developed to identify (i) the influence of low temperature (−40 °C) during ML testing, as well as (ii) the effect of accelerated temperature cycling (ATC) – 50 cycles between −40 °C and +110 °C – prior to ML testing at 25 °C. After analyzing the results of the mini-modules under combined stress conditions, the most relevant stressors were identified. This advanced test matrix therefore mimics stressors of the cold and snowy climate, such as temperature fluctuations prior to snow or wind loads, and subzero temperatures during the loads. In total, three distinct test sequences were evaluated (Fig. 6):

- ML test at 25 °C after thermal cycling: ML test was conducted following 50 accelerated thermal cycles (ATC) – between −40 °C and +110 °C – as part of a broader stress sequence, which included subsequent 4 humidity freeze cycles. The temperature was increased to 110 °C to enhance the stress on the module laminate, according to IEC 62892:2019.[16]
- ML test at −40 °C: performed inside a climate chamber to assess the direct influence of low temperatures on mechanical stability.
- ML test at 25 °C (reference): conducted without prior thermal preconditioning to serve as a baseline.

To ensure uniform pressure application during the ML tests, the load was applied using two large sand-filled bags. The weight of each bag was adjusted based on the contact area and the target pressure for the test. These were lifted and placed slowly and evenly using a forklift truck, minimizing the risk of unintentional damages (Fig. 7). Each mechanical load test sequence consisted of three steps:

1. Pre-test: A pressure of 2400 Pa was applied, followed by evaluation using EL imaging.
2. Main test: A pressure of 5400 Pa was applied to simulate a high snow load, followed by evaluation using EL imaging.
3. Wind simulation: A pressure of −2400 Pa was applied to the rear side of the module, with a final EL image taken afterwards.

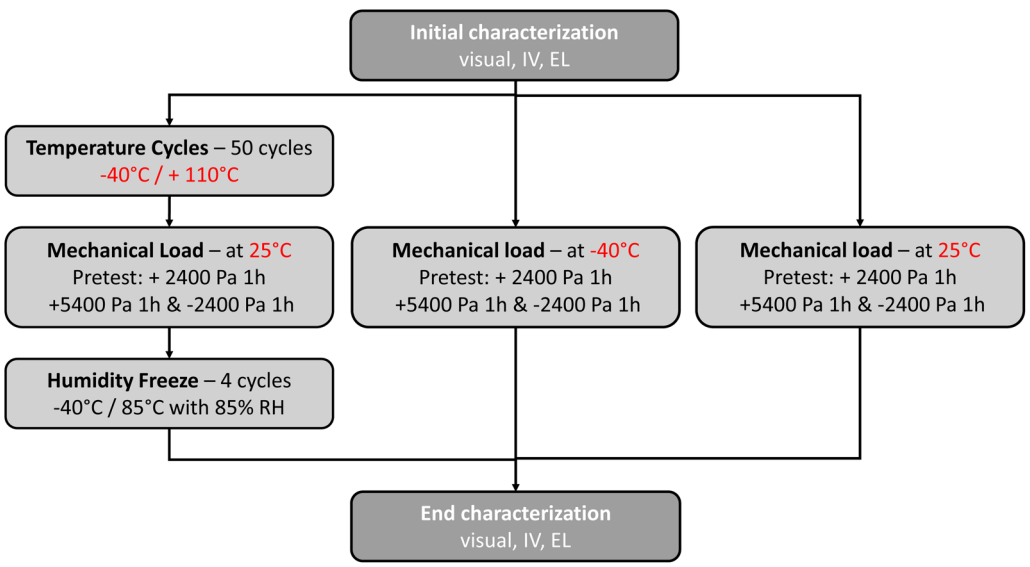

Fig. 6 Developed test sequences used on full-size modules to determine the influence of low temperatures and pre-stress (accelerated temperature cycles) on the mechanical stability.

Fig. 7 Setup for the mechanical load testing in the climate chamber. The weight was evenly distributed with sand-filled bags.

At the beginning and end of the test, visual inspection, electrical performance (*I–V* curves) and EL measurements were conducted to detect relevant failure modes. The deflection of the modules during the loading was measured with a digital laser distance meter Zamo from Bosch with an accuracy of 2 mm.

3 Results and discussion

3.1 Material tests

Encapsulants play a critical role in protecting solar cells from various environmental stressors, including mechanical loads. This is achieved by choosing a polymer encapsulant that has flexible properties at standard operating temperatures of the modules. However, when the temperatures drop below their T_g and the polymer turns into a glassy state, protection of cells against mechanical impacts (*e.g.*, snow and wind loads) is limited.[1,19] As a first step, the T_g of four different encapsulation materials currently used in PV-industry was determined using DSC. These measurements resulted in characteristic glass transition values of −30 °C for EVA, −50 °C for POE, and −122 °C for silicone. EPE, which has a layered structure consisting of EVA and POE, exhibited two distinct glass transitions at −30 °C and −50 °C, respectively. Similar values for EVA and POE have been published in the literature, although the exact values depend on the specific method and device used.[27,28] It should be noted that the glass transition is not a single point, but rather a range with an onset of the curve typically 10 °C higher than the transition point. Therefore, the EVA and EPE begin to change at −20 °C, and the POE at −40 °C. Additionally, the glass transition can be measured using other methods, such as rheology or DMA. In this case, the focus is on the material's flow behavior, and higher values are measured. The DMA analysis conducted in this study, resulted in temperatures of the maxima in the dissipation factor, of around −14 °C for EVA, −31 °C for POE and −15 °C for EPE, well aligned with the literature.[19,27,29] As module temperatures of −20 °C or −30 °C can be reached in PV systems installed at high altitudes[3] or latitudes, this is below the mechanically derived glass transition of EVA or EPE. These results already provide valuable information about the potential applicability of modules with different encapsulation materials at low temperatures. They were subsequently confirmed by further mechanical testing.

Fig. 8a compares the tensile stress of the same four types of encapsulants as described before at 10% elongation and temperatures between +50 and −40 °C. The results demonstrate the good low-temperature behavior of POE and specifically of silicone which retains its flexible properties even at low temperatures. In contrast, both EVA and EPE exhibit significantly increased tensile stress when tested at/below −20 °C, indicating a transition to a stiffer state. This is in good agreement with the discussed T_g values obtained upon measurements with DMA. The change in the polymer state is also visible in the differences between the tensile strength curves measured at 23 °C and −40 °C. At room temperature, EVA, POE, and EPE exhibit the typical curve of a soft and elastic polymer. However, at −40 °C, the EVA (and EPE to a lesser extent) curves change to the characteristic shape of a hard/though polymer (Fig. 8b).

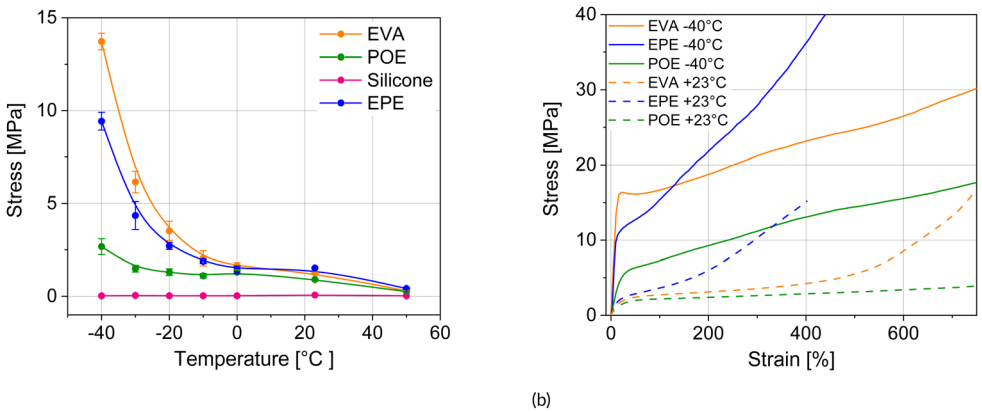

Fig. 8 (a) Curves resulting from tensile stress tests: Stress at 10% elongation of encapsulants at varying temperatures. (b) Tensile strength curves of EVA, POE and EPE at −40 °C (solid lines) and +23 °C (dashed lines).

3.2 Mini modules

3.2.1 Results of the dynamic mechanical load test. To understand the impact of encapsulation material properties on the mechanical stability of the module assembly, specific accelerated aging test sequences were developed. Dynamic mechanical loading (DML) has been found to be the most significant trigger for the formation of defects and subsequent electrical degradation, especially when the DML test is performed after a previously applied thermal cycling stress.[22,23] 4-Cell mini modules with G/G and G/BS structure were subjected to four cycles of an accelerated aging test sequence, as described in Section 2.2.1. After each cycle of the test sequence, EL images were taken and the newly developed failures in the solar cells (cell cracks, microcracks and solder bond damage) were counted (Fig. 10a). It shows that the G/G structure prevents the formation of new cell cracks upon DML application. In contrast, most of the G/BS samples started to crack upon DML-testing.

The deflection of the modules was measured during the DML test. The results show that the G/G module was deflected by 0.34 mm, compared to 0.74 mm of the G/BS modules, with identical front glass thickness. This confirms that modules with two panes of glass – of the same thickness – provide better protection for encapsulated cells under mechanical stress when the module structures are otherwise identical. Furthermore, due to the symmetrical G/G structure, the cells are located in the neutral axis of the laminate. According to finite element simulations (FEM) in the relevant literature, cells in this position are subjected to significantly lower stresses.[25,30] The EL images depicted in Fig. 9 show several failures after the four cycles of testing. Cell cracks, micro cracks and solder bond issues are visible. The images as well as the results of the cell crack counts given in Fig. 10a reveal that the mini modules containing EVA encapsulants were more prone to cell cracking and solder bond issues than those with POE encapsulation, which is consistent with the material characteristics at low temperatures. The cracks in the cells increase the series resistance, which decreases the fill factor (FF) of the IV curve indicating power loss of the module. The higher number of cracks in the EVA mini modules resulted in a more significant decrease in the FF of −4% and −6% compared to −2% and −5% for the POE mini modules. As expected, this reduction in FF impacted the electrical performance at the maximum power point (P_m) of the mini modules (Fig. 9). Contrary to the encapsulant, the type of backsheet material (PET or Tedlar) had no effect on the extent of cell cracking. The DML tests gave interesting results regarding the impact of encapsulant material type and module structure on the module stability under dynamic stress *e.g.*, wind load. Next, static load tests were performed to mimic high snow loads on the modules.

3.2.2 Results of the static mechanical load test. To asses the influence of module configuration and encapsulation material on cell crack formation and propagation under static mechanical loading at low temperatures, a static load was applied using a three-point bending setup within a climate chamber, as described in Section 2.2.2. The temperature was decreased in steps of 10 °C and at each step load was applied for one hour. Fig. 10b shows the temperature at which initial cell cracking was observed in the different samples. Again, the results indicate that G/G mini modules exhibit significantly higher resistance to cell cracking compared to G/BS mini modules. Furthermore, the experiment supports earlier findings, that G/BS mini modules with EVA encapsulation are more prone to cell cracking than those encapsulated with POE, and highlights the superior low-temperature mechanical stability of POE-based modules.

3.3 Full-size module testing

Further experiments were carried out on full-size PV modules to validate and extend the findings of the mini module tests. These tests aimed to assess whether the trends observed in mini

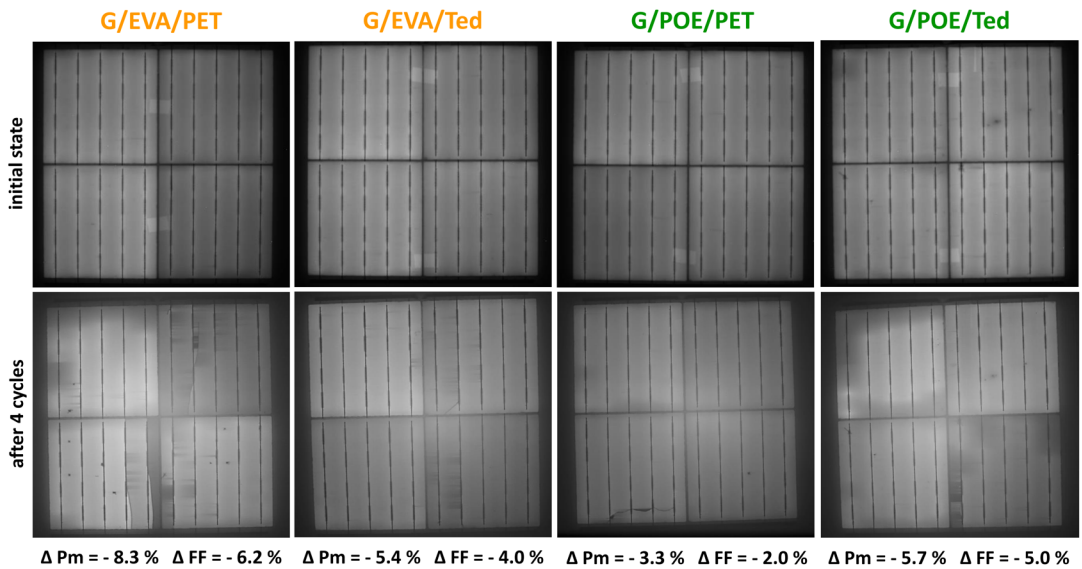

Fig. 9 EL images of G/BS mini modules at the initial state (top) and after the fourth cycle of the test sequence (bottom). (Micro-) cell cracks and solder bond failures developed during the four cycles. FF: fill factor, P_m: power at maximum power point.

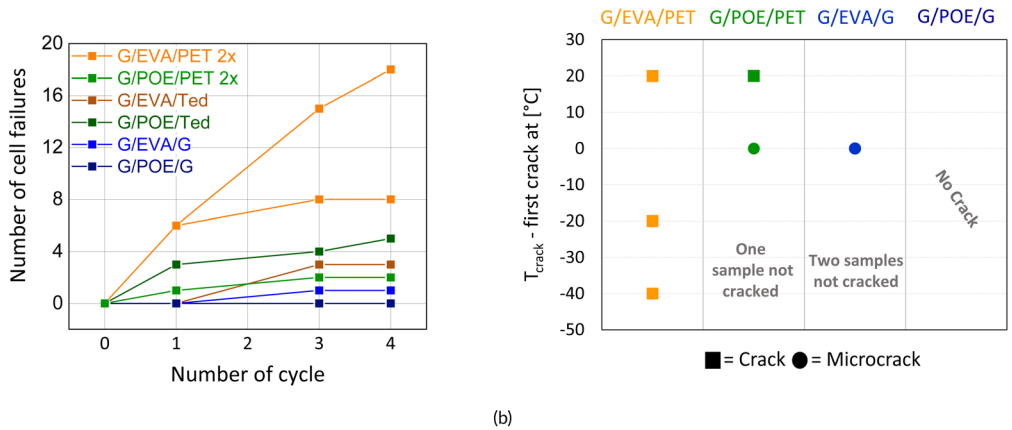

Fig. 10 (a) Number of failures (cell cracks, micro cracks and solder bond failures) in the eight mini modules after each cycle of the accelerated test sequence including dynamic mechanical loading. (b) Temperature at which the first cell (micro-) cracks appeared during the static mechanical load while temperature was decreased in steps.

modules would hold in full-size PV modules. Testing full-size modules is important because module size and mounting conditions can significantly impact mechanical load distribution and failure modes, which mini modules do not capture.

3.3.1 Glass/backsheet modules. For the G/BS modules with PERC cells and busbar metallization, the three test sequences (see Fig. 6) resulted in the formation of cell cracks of varying severity. Initial cell cracks were identified in the EL images after applying a ML of +2400 Pa. However, cracks were only observed in the modules where (i) the load was applied at −40 °C and (ii) the load was applied at 25 °C after pre-stressing with ATC. These cracks propagated further under subsequent application of a +5400 Pa load (Table 2). Notably, the module that underwent temperature cycling before ML exhibited cracks in nearly all cells, displaying the characteristic X-pattern of cracking associated with high mechanical stress for PV modules with a frame. Subsequent humidity freeze cycles did not result in the formation of additional cracks. In contrast, the module tested with ML at 25 °C without pre-stressing showed only two minor cracks. It should be mentioned that some modules developed small cracks during the manufacturing process. However, these cracks did not affect the test results. EL images of the initial state are presented in the Appendix (Fig. 12).

The electrical results are consistent with the observations in the EL images (Table 2). The module that underwent the *ATC-ML-humidity freeze* test sequence exhibited the highest power degradation, with a P_m reduction of −9.1%, mostly due to a FF losses of −4.1%. The module tested at −40 °C for ML exhibited a P_m loss of −6.0% (ΔFF = −1.9%), while the module tested for ML at 25 °C (the reference condition), which did not show significant cracking, exhibited the lowest loss of P_m = −2.5% (ΔFF = −0.1%). The power loss in the absence of visible cracking is most likely attributed to metastability effects of the module.

The results clearly show that the stiffness of the encapsulation material at temperatures below its glass transition significantly affects the outcome of the static mechanical load test. This becomes evident when comparing the ML test results at −40 °C and +25 °C of full-size modules with PERC cells and five busbars. The higher number of cell cracks in the module tested at −40 °C also resulted in higher power degradation. This underscores the importance of testing modules at temperatures comparable to those experienced under real-world conditions to simulate failures that also occur in field installations. However, most cracks were observed in the ML test following ATC. This suggests that the mismatch in the coefficients of thermal expansion of the different module materials plays a critical role. In the applied test sequence, this impact was reinforced by the intensified TC-parameters of −40 °C to +110 °C. Since the encapsulant is compressed above the busbars, shrinkage is less there than in the encapsulant to the left and right of the busbar (see Fig. 11 left). For this reason, stress is applied to the cell in this area during the transition to lower temperatures, which can cause microcracks beneath the busbar. These microcracks are not visible in the EL images after ATC but grow into larger, detectable cracks after ML.[22,31]

After conducting additional tests on G/BS modules with TOPCon cells and multi-wire connection technology, the explanation of the crack formation mechanism was supported. Due to the different dimensions of the round multi-wires and their smaller contact area with the solar cell (Fig. 11 right), stress on the cells during ATC is significantly lower. The wires displace significantly less encapsulant material than the broader busbars (four times broader). As a result, only a few cell cracks or damages were detected in the wired half-cut TOPCon cells encapsulated with EVA, POE and EPE. When using multi-wire interconnections with a 250 μm diameter, no significant influence of the encapsulant type on cell resistance to static mechanical stress at low temperatures was detected. Overall, multi-wires offer better resistance to mechanical load in cold conditions compared to bulkier busbar technology, primarily due to their reduced volume.

The results of the EL images of G/BS modules after ML tests (Table 2) indicate that the stress impact applied in the three different test sequences (shown in Fig. 6) yields significantly different levels of degradation in modules with busbar

Table 2 EL images of full-size G/BS modules during and after the three different ML test sequences. Difference in severeness of cell cracking is visible and also reflected in the power (P_m) and fill factor (FF) loss. EL images of the initial state are presented in the Appendix, where only small failures from production are visible

	TC - > ML at 25 °C	ML at −40 °C	ML at 25 °C
TC50	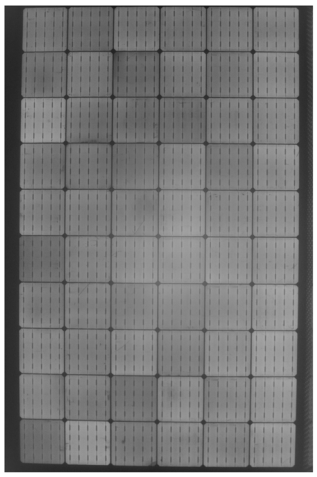	Not applicable	Not applicable
	No new cell cracks	No cell cracks	No cell cracks
+2400 Pa	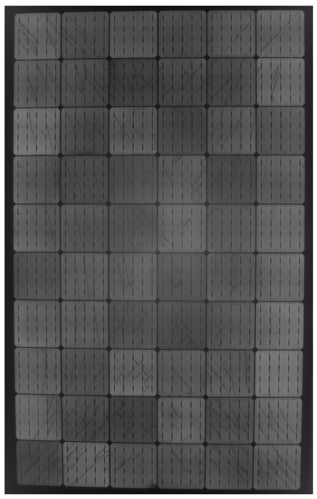	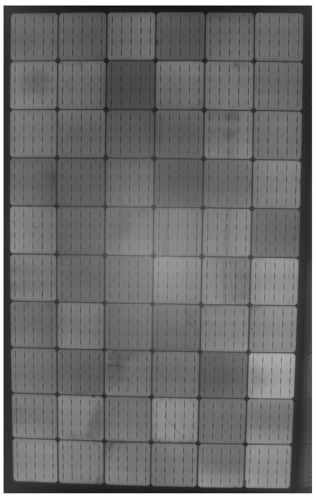	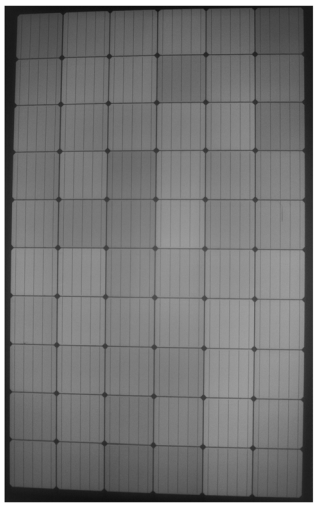
	Severe cell cracks	First single cell cracks	No cell cracks
+5400 Pa	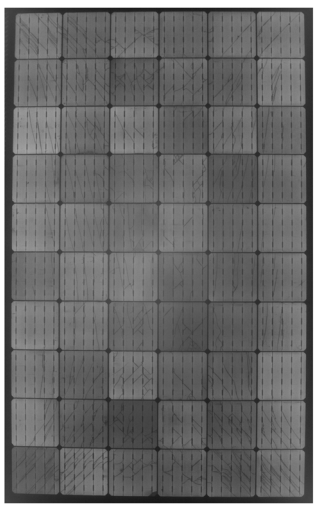	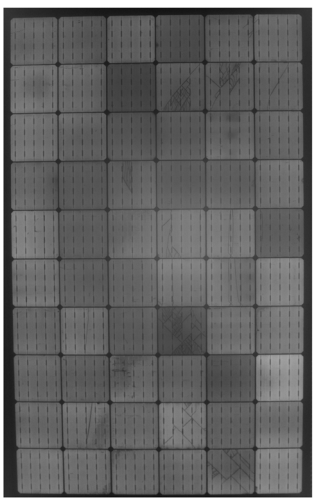	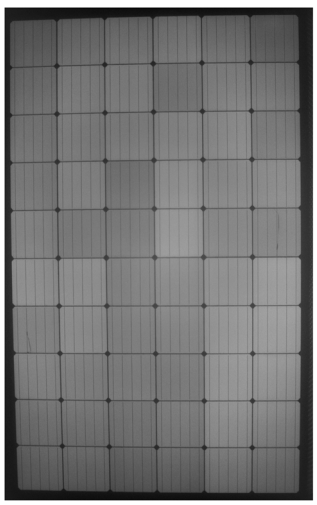
el. deg.	Severe cell cracks expanded $\Delta P_m = -9.1\%$; $\Delta FF = -4.1\%$	Several cell cracks $\Delta P_m = -6.0\%$; $\Delta FF = -1.9\%$	2 small cell cracks $\Delta P_m = -2.5\%$; $\Delta FF = -0.1\%$

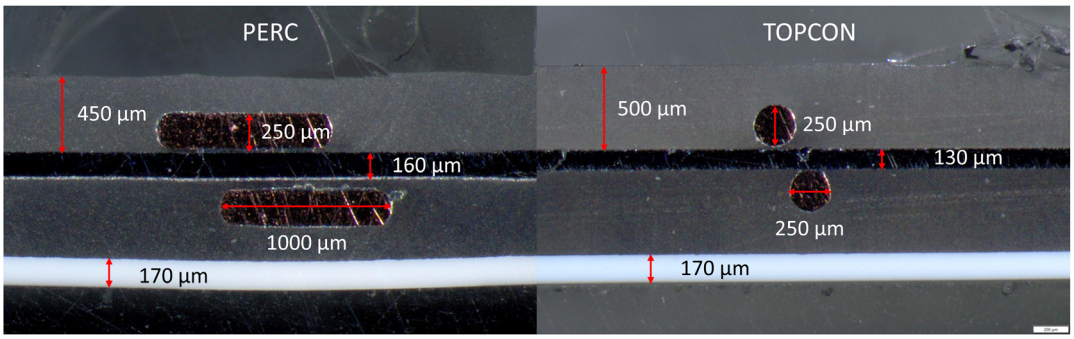

Fig. 11 Light microscopic image of cross sections of G/BS modules comparing PERC cells with busbars (left) and TOPCon cells with multi-wires (right).

metallization. One conclusion that can be drawn from these results is that the standard stress test should be modified for modules intended for use in regions with temperatures below freezing. The effect of low temperatures on the mechanical robustness of the modules must be taken into account. However, this would require a longer test duration or the use of specialized laboratory equipment (*e.g.*, a climate chamber large enough to accommodate the stress test apparatus). Since the stress test at 25 °C after the ATC exhibits the same failure mechanism as the ML test at −40 °C (albeit to a greater extent), it could serve as a practical alternative to the stress test at −40 °C. This approach is also easier to implement, as it can be carried out in most laboratories.

3.3.2 Glass/glass modules. The application of the three different test strategies (Fig. 6) did not induce any cell cracks in the G/G modules under test, although they had the same PERC cell matrix and EVA encapsulant as the PERC G/BS modules described above. The absence of cell cracks also resulted in no noticeable change in electrical power upon these tests. However, glass breakage occurred at higher loads, especially in modules with thinner glass (2 × 3 mm and 2 × 4 mm). Due to the frameless design, the clamping area was the weak point in the mechanical test. The module with 2 × 3 mm glass broke at 5400 Pa, while the module with 2 × 4 mm glass broke at an increased load of 6400 Pa. During the ML test, the structural support of the frame was missing for the G/G modules. This resulted in a maximum deflection of around 3 cm in the middle of the G/G module (2 × 4 mm), similar to that of the G/BS module with 1 × 4 mm glass. However, the bending formation changes depending on whether a frame is used or not. Since the frameless G/G modules were only mounted along the long side (with three clamps each), the deflection resembled a cylinder, with 3 cm of deflection along most of the middle axis. It is assumed that this type of bending exerts less stress on the solar cells than bending of a framed module which takes the form of an ellipsoid upon load and the diagonals bear most of the pressure — which explains the X-shaped crack pattern.[32] Additionally, FEM modeling of Beinert *et al.*[25] and Gabor *et al.*[30] showed that, due to the symmetrical structure of the G/G modules, the cells are in the neutral axis and therefore experience much less stress, which explains the absence of cell cracks in the mechanical load testing in this study.

4 Conclusions

This study systematically investigated the mechanical stability of PV modules under static and dynamic loads at varying temperatures, with a particular focus on encapsulant type and module configuration. Material and mini-module tests revealed that encapsulant choice significantly impacts mechanical stability at low temperatures. The use of POE as an encapsulant outperformed the use of EVA in both static and dynamic load testing of mini modules, especially at sub-zero temperatures. The DSC and DMA analyses revealed that POE has a glass transition temperature of −50 °C (DSC) or −31 °C (DMA), which is significantly lower than that of EVA, which is −30 °C or −14 °C. This lower glass transition enables POE to retain its flexibility at lower temperatures, providing a material advantage that directly contributes to improved module performance. POE-based mini modules exhibited fewer cell failures which resulted in lower fill factor and power losses, after a test sequence including dynamic mechanical loading. In contrast, G/BS modules with EVA were more susceptible to cracking at low temperatures or after thermal preconditioning due to encapsulant stiffening and the structure's lower inherent rigidity, resulting in a higher fill factor and power degradation. Using both mini and full-size modules, it was demonstrated that G/G module architectures offer superior mechanical stability for the solar cells compared to G/BS configurations. The G/G structure minimized cell crack formation during dynamic and static mechanical load tests. However, the frameless design of the full-size G/G modules causes issues at higher loads, as robust mounting on frameless modules is difficult. Glass breakage occurred with the 2 × 3 mm G/G module at 5400 Pa and with the 2 × 4 mm module at 6400 Pa. This underlines the importance of robust module designs with sufficient glass thickness and a frame that enables efficient mounting to withstand the higher loads in cold and snowy climates. The recent industry trend towards modules with thinner glass panes is not suitable for application in this harsh climate. In areas where higher mechanical loads are expected, the modules, structure, and mounting must be chosen wisely and tested accordingly. However, optimizing and testing different mounting configurations was not part of this study. In future work, further testing would be required to compare the number

and position of clamps on framed and unframed modules and their effect on glass breakage and cell cracking.

G/BS full-size modules could withstand higher loadings due to their reinforced frames. However, in full, busbar-connected PERC cells, cell cracking occurred. The highest number of cracks and the resulting highest electrical degradation ($P_m = -9.1\%$, FF $= -4.1\%$) occurred through the test sequence comprising accelerated thermal cycling (−40°C/+110 °C), prior to ML and humidity freeze cycles. In addition, ML tests at −40 °C also caused several cell cracks and a degradation of ($P_m = -6.0\%$), while tests at 25 °C without thermal preconditioning resulted in no severe cracking or significant electrical degradation within measurement uncertainties. Further tests demonstrated that modern module designs, with half-cut and thinner cells, as well as round multi-wires, help to prevent cell cracking at ML at or after low temperature exposure. After all three test sequences of the ML test, EL images revealed only single cracked cells, with no significant difference observed between these modules tested at different temperatures or after preconditioning. Notably, also no visible cell cracks or electrical losses were observed in any G/G modules, regardless of the test sequence.

In general, the results emphasize the importance of adapting testing strategies to the specific climate and stress factors present at the installation site of the modules. Clear differences were found between standard mechanical load tests at room temperature – as performed during the certification process according to IEC 61215 – and adapted tests involving low temperatures, which resembles real outdoor stressors in cold and snowy climates more closely. For some module designs, cell cracking increased significantly when a load was applied at a low temperature or after temperature cycles. Both of these tests produced similar types of cell cracks along the diagonals of the modules, starting at the busbars. In cases where a mechanical load test at low temperatures is logistically challenging or not feasible, similar failure modes can be induced by performing temperature cycles prior to a mechanical load test at room temperature.

The results underscore the importance of encapsulant selection and optimized module structures to ensure long-term mechanical durability of PV modules in cold and snowy environments, where mechanical stress, low temperatures, and temperature fluctuations are common stressors. G/G modules with POE encapsulation and multi-wire metallization provide the best mechanical protection for PV cells when combined with an robust frame and optimizing clamping. These findings offer valuable insights to manufacturers seeking to improve module resilience in cold and snowy climates.

Author contributions

Anika Gassner: conceptualisation, methodology, investigation, formal analysis, visualisation, writing – original draft, writing – review & editing. Gabriele C. Eder: conceptualisation, methodology, writing – review & editing, supervision. Ebrar Özkalay: conceptualisation, methodology, formal analysis, writing – review & editing. Gabi Friesen: conceptualisation, writing – review & editing. Markus Feichtner: conceptualisation, resources. Vasiliki-Maria Archodoulaki: writing – review & editing, supervision.

Conflicts of interest

There are no conflicts of interest to declare.

Data availability

Data for this article, including differential scanning calorimetry (DSC), dynamic mechanical analysis (DMA), and electroluminescence (EL) images are archived and available in Zenodo with the DOI: **https://doi.org/10.5281/zenodo.16739091**.

Appendix

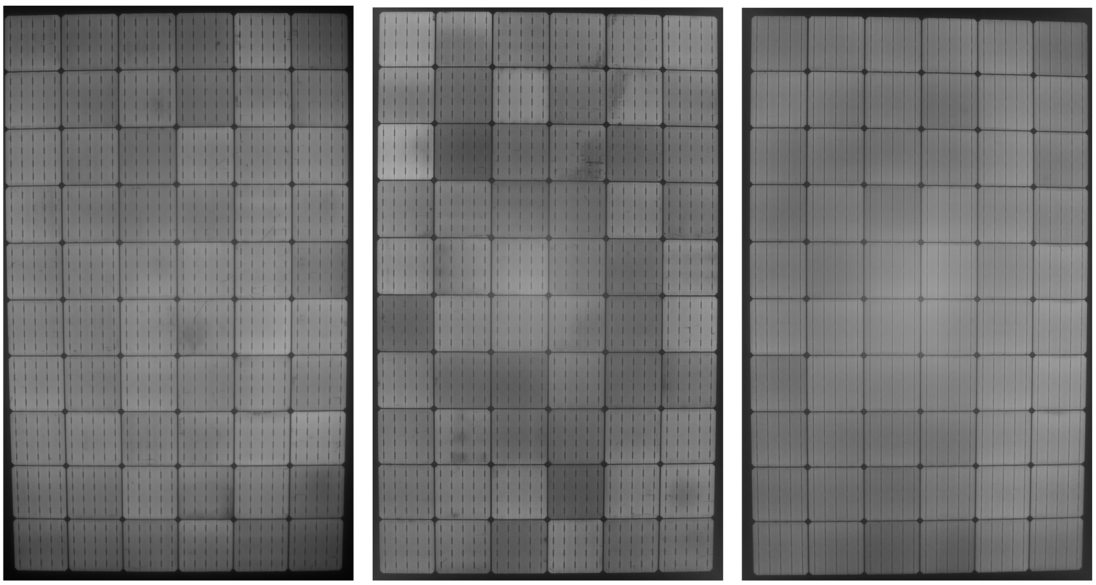

(a) Module for TC -> ML at -25°C (b) Module for ML at -40°C (c) Module for ML at 25°C

Fig. 12 (Appendix) Initial EL of full-size G/BS modules with PERC cells. Some small failures are visible from the production.

Acknowledgements

The work was supported by Climate and Energy fund processed by the Austrian Research Promotion Agency (FFG) and the Swiss Federal Office of Energy (SFOE) within the Solar-Era. net project PV-DETECT, under agreement numbers FO999897441 and SI/502484-1, respectively. The authors want to thank their colleagues from OFI, most of all Simeon Morariu, but also David Orsovanovic, Franz Burger and Philipp Larisch for the help during the mechanical load testing. Without them, the experiments could not have been conducted that way. Also they would like to thank Moreno Ronchi from SUPSI for generously sharing his valuable expertise in conducting the mechanical load test for this work. Our thanks further go to colleagues at the SUPSI – Flavio Valoti, Mattia Ceretti, and Boris Margna – for performing the electrical characterization.

References

1 G. Friesen, L. Micheli, G. C. Eder, T. Müller, J. M. Y. Ali and M. Rivera, *et al.*, *Optimisation of Photovoltaic Systems for Different Climates*, 2025, pp. T13-32, https://iea-pvps.org/key-topics/t13-optimisation-pv-systemsdifferent-climates-2025/.

2 D. Anderegg, S. Strebel and J. Rohrer. *Photovoltaik Versuchsanlage Davos Totalp Messergebnisse Winterhalbjahr 2020/2021. ZHAW Züricher Hochschule für Angewandte Wissenschaften*; IUNR Institut für Umwelt und Natürliche Ressourcen; 2021, available from: https://digitalcollection.zhaw.ch/server/api/core/bitstreams/ee0f69fc-dd97-48a3-a536-aa6757b87601/content.

3 E. Özkalay, H. Quest, A. Gassner, A. Virtuani, G. C. Eder, S. Vorstoffel, *et al.*, Three decades, three climates: environmental and material impacts on the long-term reliability of photovoltaic modules, *EES Sol.*, 2025, **1**, 580–599, available from: https://xlink.rsc.org/?DOI=D4EL00040D.

4 A. Mellot, C. Moretti, T. Tröndle and A. Patt, Mitigating future winter electricity deficits: A case study from Switzerland, *Energy Convers. Manage.*, 2024, **309**, 118426, available from: https://www.sciencedirect.com/science/article/pii/S0196890424003674.

5 A. Kahl, J. Dujardin and M. Lehning, The bright side of PV production in snow-covered mountains, *Proc. Natl. Acad. Sci. U. S. A.*, 2019, **116**(4), 1162–7. Publisher: Proceedings of the National Academy of Sciences, available from: https://www.pnas.org/doi/10.1073/pnas.1720808116.

6 Association SEI. Alaska: State Overview, available from: https://seia.org/state-solar-policy/alaska-solar/.

7 M. Formolli, T. Kleiven and G. Lobaccaro, Assessing solar energy accessibility at high latitudes: A systematic review of urban spatial domains, metrics, and parameters, *Renewable Sustainable Energy Rev.*, 2023, **177**, 113231, available from: https://www.sciencedirect.com/science/article/pii/S1364032123000874.

8 M. Koehl, M. Heck and S. Wiesmeier, Categorization of weathering stresses for photovoltaic modules, *Energy Sci. Eng.*, 2018, **6**(2), 93–111, available from: https://onlinelibrary.wiley.com/doi/10.1002/ese3.189.

9 M. Halwachs, L. Neumaier, N. Vollert, L. Maul, S. Dimitriadis, Y. Voronko, *et al.*, Statistical evaluation of PV system performance and failure data among different climate zones, *Renewable Energy*, 2019, **139**, 1040–1060, available from: https://linkinghub.elsevier.com/retrieve/pii/S0960148119303003.

10 A. Omazic, G. Oreski, M. Halwachs, G. C. Eder, C. Hirschl, L. Neumaier, *et al.*, Relation between degradation of polymeric components in crystalline silicon PV module and climatic conditions: A literature review, *Sol. Energy Mater. Sol. Cells*, 2018, **192**, 123–133, available from: https://linkinghub.elsevier.com/retrieve/pii/S0927024818305956.

11 K. A. Weiß, E. Klimm and I. Kaaya, Accelerated aging tests *vs.* field performance of PV modules, *Prog. Energy*, 2022, **4**(4), 042009, available from: https://www.iopscience.iop.org/article/10.1088/2516-1083/ac890a.

12 B. F. H. ZHAW and O. S. T. SUPSI, *Alience - Alpine PV Competence*, 2025, available from: https://alpine-pv.ch/.

13 International Electrotechnical Commission, *IEC 61215–2: 2021 Terrestrial Photovoltaic (PV) Modules - Design Qualification and Type Approval - Part 2: Test Procedures*, 2021, available from: https://www.webstore.iec.ch/en/publication/61350.

14 International Electrotechnical Commission, *IEC 61730-2:2023 Photovoltaic (PV) Module Safety Qualification - Part 2: Requirements for Testing*, 2023, available from: https://webstore.iec.ch/en/publication/63895.

15 Commission IE, *IEC TS 63126:2020 Guidelines for Qualifying PV Modules, Components and Materials for Operation at High Temperatures*, 2020, available from: https://webstore.iec.ch/en/publication/59551.

16 Commission IE, *IEC 62892:2019 Extended Thermal Cycling of PV Modules - Test Procedure*, 2019, available from: https://webstore.iec.ch/en/publication/29329.GASSNERetal.21.

17 Commission IE, *IEC 62938:2020 Photovoltaic (PV) Modules - Non-uniform Snow Load Testing*, 2020, available from: https://webstore.iec.ch/en/publication/33027.

18 Commission IE, *IEC TS 63397:2022 Photovoltaic (PV) Modules - Qualifying Guidelines for Increased Hail Resistance*, 2022, available from: https://webstore.iec.ch/en/publication/68735.

19 P. Romer, K. B. Pethani and A. J. Beinert, Effect of inhomogeneous loads on the mechanics of PV modules, *Prog. Photovolt.: Res. Appl*, 2024, **32**(2), 84–101, available from: https://www.onlinelibrary.wiley.com/doi/abs/10.1002/pip.3738.

20 G. W. Ehrenstein, *Polymeric Materials: Structure – Properties – Applications*, Carl Hanser Verlag GmbH & Co. KG, München, 2001, available from: https://www.hanser-elibrary.com/doi/book/10.3139/9783446434134.

21 A. Granlund, M. Lindh, T. Vikberg and A. M. Petersson, Evaluation of Snow Removal Methods for Rooftop Photovoltaics, *8th World Conference on Photovoltaic Energy*

Conversion, 2022, 1122–1128, available from: https://userarea.euovsec.org/proceedings/WCPEC-8/4DO.4.6/.

22 M. W. Rowell, S. G. Daroczi, D. W. J. Harwood and A. M. Gabor, The Effect of Laminate Construction and Temperature Cycling on the Fracture Strength and Performance of Encapsulated Solar Cells, in *7th World Conference on Photovoltaic Energy Conversion (WCPEC)*, IEEE, Waikoloa Village, HI, 2018, pp. 3927–31, available from: https://ieeexplore.ieee.org/document/8547978/.

23 E. J. Schneller, H. Seigneur, J. Lincoln and A. M. Gabor, The Impact of Cold Temperature Exposure in Mechanical Durability Testing of PV Modules, in *2019 IEEE 46th Photovoltaic Specialists Conference (PVSC)*, IEEE, Chicago, IL, USA, 2019, pp. 1521–4, available from: https://ieeexplore.ieee.org/document/8980533/.

24 A. MHG, *Solar Simulation | Solar Simulation Weathering | Atlas*, available from: https://www.atlas-mts.com/products/custom-solar-simulation/mhg-solar-simulation.

25 A. J. Beinert, P. Romer, M. Heinrich, M. Mittag, J. Aktaa and D. H. Neuhaus, The Effect of Cell and Module Dimensions on Thermomechanical Stress in PV Modules, *IEEE J. Photovolt*, 2020, **10**(1), 70–77, available from: https://ieeexplore.ieee.org/document/8901435.

26 Sonnenkraft-Energy-GmbH, *Datenblatt-POWER-Modul ALPIN*, available from: https://www.sonnenkraft.com/files/sonnenkraft/05_Downloadbereich/Produkte/Module/04_hohe_Schneelasten/Datenblatt-fuer-hohe-SchneelastenPOWER-ALPIN_325_430.pdf.

27 M. D. Kempe, G. J. Jorgensen, K. M. Terwilliger, T. J. McMahon, C. E. Kennedy and T. T. Borek, Acetic acid production and glass transition concerns with ethylene-vinyl acetate used in photovoltaic devices, *Sol. Energy Mater. Sol. Cells*, 2007, **91**(4), 315–329, available from: https://www.sciencedirect.com/science/article/pii/S0927024806004107.

28 N. T. Dintcheva, E. Morici and C. Colletti, Encapsulant Materials and Their Adoption in Photovoltaic Modules: A Brief Review, *Sustainability*, 2023, **15**(12), 9453, available from: https://www.mdpi.com/2071-1050/15/12/9453.

29 K. Agroui, G. Collins and J. Farenc, Measurement of glass transition temperature of crosslinked EVA encapsulant by thermal analysis for photovoltaic application, *Renewable Energy*, 2012, **43**, 218–223, available from: https://www.linkinghub.elsevier.com/retrieve/pii/S0960148111006173.

30 A. Gabor, R. Janoch, A. Anselmo, J. Lincoln, H. Seigneur and C. Honeker, Mechanical load testing of solar panels — beyond certification testing, in *43rd IEEE Photovoltaic Specialist Conference*, 2016, pp. 3574–9.

31 H. Seigneur, E. Schneller, J. Lincoln, H. Ebrahimi, R. Ghosh, A. M. Gabor, *et al.*, Microcrack Formation in Silicon Solar Cells during Cold Temperatures, in *2019 IEEE 46th Photovoltaic Specialists Conference (PVSC)*, IEEE, Chicago, IL, USA, 2019, pp. 1–6, available from: https://www.ieeexplore.ieee.org/document/9198968/.

32 S. Kajari-Schröder, I. Kunze, U. Eitner and M. Köntges, Spatial and orientational distribution of cracks in crystalline photovoltaic modules generated by mechanical load tests, *Sol. Energy Mater. Sol. Cells*, 2011, **95**(11), 3054–3059, available from: https://www.sciencedirect.com/science/article/pii/S0927024811003710.